

Fluorescence Molecular Tomography Based on *a priori* Information

Ahmed Serdaroglu and Birsen Yazici

Department of Electrical, Computer, and Systems Engineering, Rensselaer Polytechnic Institute, 110 8th Street, Troy, New York 12180
serdaa2@rpi.edu

Vasilis Ntziachristos

Center for Molecular Imaging Research, Department of Radiology, Massachusetts General Hospital, Harvard Medical School, Charlestown, Massachusetts 02129

Abstract: We obtain fluorophore absorption reconstructions from small animals *in-vivo* by incorporating *a priori* anatomical information obtained from Magnetic Resonance Imaging into the optical measurements. The mismatch between the anatomical and functional images is accounted by using a Tikhonov-based regularization approach. © 2006 Optical Society of America
OCIS codes: (170.3010) Image reconstruction techniques; (170.3880) Medical and biological imaging

1. Introduction

Optical macroscopic imaging of cellular and sub-cellular activity in biological media is an emerging modality. Particular attention has been given to the use of near-infrared (NIR) fluorescent probes in order to achieve high detection sensitivity and to the implementation of Fluorescence Molecular Tomography (FMT) to enable accurate and quantitative imaging of protein concentration, function and gene expression in vertebrates *in-vivo* [1]. Largely, based on solutions developed for photon propagation in highly scattering media [2], FMT utilizes the coupled diffusion equations to define the propagation of excitation light in the diffuse medium and the emission light from the fluorophores to the detectors on the boundary. In FMT systems, the localization and quantification of pathological diseases are achieved by generating 3D images of spatially varying absorption of endogenous and exogenous chromophores, from the measurements obtained at both the excitation and emission wavelengths separated by spectral filtering at the detector sides [3]. The inverse problem in this case is ill-posed, and needs regularization in order to achieve stable solutions, albeit with reduced resolution. Original FMT systems yielded undetermined inversion schemes, however recent technological advances using noncontact measurements and direct coupling of CCD cameras offer high information data sets and measurements that reach well above 10^8 [4-6]. A promising approach to the regularization of the inverse problem is the use of *a priori* information provided by an anatomical imaging modality such as Magnetic Resonance Imaging (MRI). Solutions utilizing *a priori* information in diffusive inverse problems have been previously applied for the ordinary Diffuse Optical Tomography (DOT) where the optical properties of only the endogenous chromophores are reconstructed [7-11]. Other than MRI, X-ray [12], positron emission tomography [13], and ultrasound [14] systems are also used concurrently with NIR optical imaging modalities. The anatomical information can be incorporated into the forward and/or inverse problem formulations of the FMT model. The incorporation of the prior information into the forward problem can be achieved by defining the discretization of the domain according to the regions recovered by segmenting the high-resolution anatomical images [15,16]. When the prior anatomical information is used in the inverse problem step to constrain the parameter updates, the ill-posed nature of the model can be reduced in great extent.

In a recent simulation study [17], the prior information was incorporated by defining Region of Interests (ROIs) according to the anatomical image which causes the spatial distribution of the fluorophore concentration and lifetime parameters to be directly determined by the pre-defined anatomical regions. In this work, different Tikhonov regularization methodologies are used in order to incorporate the *a priori* anatomical images into the optimization step of the inverse problem. The weight on optical vs. anatomical data is set by changing the regularization parameter which reduces the bias towards the anatomical information. This approach is applied to retrieving the fluorescence distribution of a fluorescent probe sensitive to major cathepsins associated with an animal model of Chronic Obstructive Pulmonary Disease (COPD), using measurements obtained *in-vivo*. Increased fluorescence is reconstructed in the lung which is consistent with an increased inflammatory response expected from this animal model and verified histologically.

2. Theory

The reconstruction of the absorption coefficient due to the fluorophores, μ_{af} , in FMT formulation is posed as an optimization problem where the error between the experimentally obtained measurements and the predicted data is

iteratively minimized with respect to μ_{af} . In this work, we add another term to the objective function to be minimized. This term, also known as the Tikhonov penalty term, is a function of the difference between the current update of the μ_{af} values at each voxel and the prior image obtained from the segmented MR images. The objective function to be minimized with respect to the image to be reconstructed can be stated as

$$C^2 = \|\mathbf{y} - \mathbf{W}\mathbf{x}\|^2 + \lambda\|\mathbf{L}(\mathbf{x} - \mathbf{x}^*)\|^2 \quad (1)$$

where \mathbf{y} is the $M \times 1$ vector which contains the emission measurements normalized with respect to the excitation measurements. This kind of normalization is proved to eliminate the source power, detector attenuation, and coupling effects which in turn lead to better reconstructions and significant insensitivity to tissue optical heterogeneity [18,19]. \mathbf{W} is the weight (or Jacobian) matrix obtained by the perturbative approach and attains similar characteristics to the Rytov approximation used for DOT. The $N \times 1$ vectors \mathbf{x} and \mathbf{x}^* correspond to the image to be reconstructed and the *a priori* image, respectively. The minimization of C^2 is performed with respect to \mathbf{x} . λ is the regularization parameter which balances the effects of anatomical and optical information. Its value can be determined experimentally, or by the L-curve approach [12]. \mathbf{L} is a regularizing matrix. In this study, we used different regularizing matrices, and compared the qualities of the reconstructed images. In particular we employed the 0th order Tikhonov regularization where \mathbf{L} was assumed as the $N \times N$ identity matrix and the 1st order Tikhonov regularization where $\mathbf{L}^T\mathbf{L}$ denotes the Laplacian such that its ij^{th} element is equal to the number of six-connected neighbors of the i^{th} voxel if $i = j$ [20]. When the j^{th} voxel is in the six-connected neighborhood of the i^{th} voxel, the ij^{th} element of $\mathbf{L}^T\mathbf{L}$ becomes -1, and zero otherwise. In addition, as a third approach, the MR segmented regions are incorporated into the regularization matrix as described in Ref. [15]. In this methodology, for each voxel, the difference between the absorption coefficients of that voxel and those that are supposed to have the same tissue type according to the segmented MR image is taken and a Laplacian-type filter smoothes the variations inside each region while preserving the edges. In this third approach, \mathbf{L}_{ij} is taken as 1 if $i = j$, $-1/N_k$ if the i^{th} and j^{th} voxels are both in the k^{th} region, and 0 otherwise. Here, N_k is the number of voxels in the k^{th} region.

3. Experimental Results

In this study, photon measurements at the excitation and emission wavelengths from Balb/c mice receiving intratracheal lipopolysaccharide (LPS) instillation of a murine model, using procedures as reported in Ref. [?], was imaged following administration of a fluorescence activatable probe sensitive to major cathepsins associated with inflammation (Prosense 680, Visen Medical, Woburn MA, excitation 672nm, emission 700-730nm). The FMT imaging setup has been previously described [5] and uses CW light, 46 sources, direct CCD camera coupling (10^6 detectors) and a slab geometry operating in limited-projection tomographic mode. The slab width was 1.3 cm. Magnetic resonance imaging was performed at 4.7T (Bruker Instruments Billerica MA). FMT and MRI imaging was performed sequentially using a rigid frame for animal translation that maintained positional accuracy to less than 1mm. The 3-D reconstructions are performed in a slab of size $3.17 \times 3.17 \times 1.3$ cm shown on the white light image of the mouse in Fig. 1(a). Extrapolated boundary conditions for the slab geometry are used in the forward model. The domain is discretized into 3600 voxels with the 3-D mesh given as $N_x = 20$, $N_y = 20$, and $N_z = 9$. 81 detector readings are taken by averaging the photon counts over the field of view extracted from the 512×512 pixels of the images acquired by the CCD camera. In order to eliminate the measurements with a low signal-to-noise ratio, thresholding is applied to the data.

The prior image is extracted by segmenting the MR images. The MR slice shown in Fig. 1(b) is a high-resolution image showing the anatomy of the animal at depth equal to 0.61 cm, and it has the same size with the imaging box shown in Fig. 1(a). A simple thresholding approach is pursued in order to segment the lungs from the background and the images are aligned using anatomical markers. The 3-D MR image is preprocessed by applying median filtering and contrast enhancement to each slice prior to segmentation. Fig. 1(c), and (d) show the corresponding slices of the preprocessed and segmented MR images, respectively. A prior fluorochrome concentration is assumed only in the lungs, and the background is assumed to have no fluorophore accumulation. A truncated conjugate gradient algorithm [11] is employed for minimizing the cost function given in Eq. (1). Figs. 1(e)-(h) show the slices of the reconstructed μ_{af} maps shown on the xy -plane at depth 0.61 cm for the different \mathbf{L} -matrices described in Section 2. The optical images are superimposed on the anatomical images. Fig. 1(e) depicts the result when no regularization is applied, i.e. for $\lambda=0$. The optimum regularization parameter was found to be 0.08 for the experiments. Figs. 1(f)-(h) show the results obtained with the 0th order Tikhonov, 1st order Tikhonov, and Tikhonov regularization where the segmented image is used to generate the regularization matrix, respectively. The effect of regularization with *a priori* information becomes obvious by these results. Better localization and contrast is obtained for the 0th order Tikhonov regularization as compared to Fig. 1(e) that did not utilize regularization. The 1st

order Tikhonov regularization leads to an even better contrast and apparent resolution. Finally, the 3rd approach described in Section 2 and shown in Fig. 1(h) does not provide as good contrast as that obtained by the 0th and 1st order Tikhonov regularization methods. It should be noted that the liver is an organ where a lot of fluorophore accumulation occurs. In prior images, we mistakenly assumed no fluorophore in the liver; yet, the algorithm is still able to reconstruct the μ_{af} due to the fluorophores in this region. This is a result that can be achieved by using soft priors. If hard priors are used, the fluorophore activity in this region is likely to be erroneous.

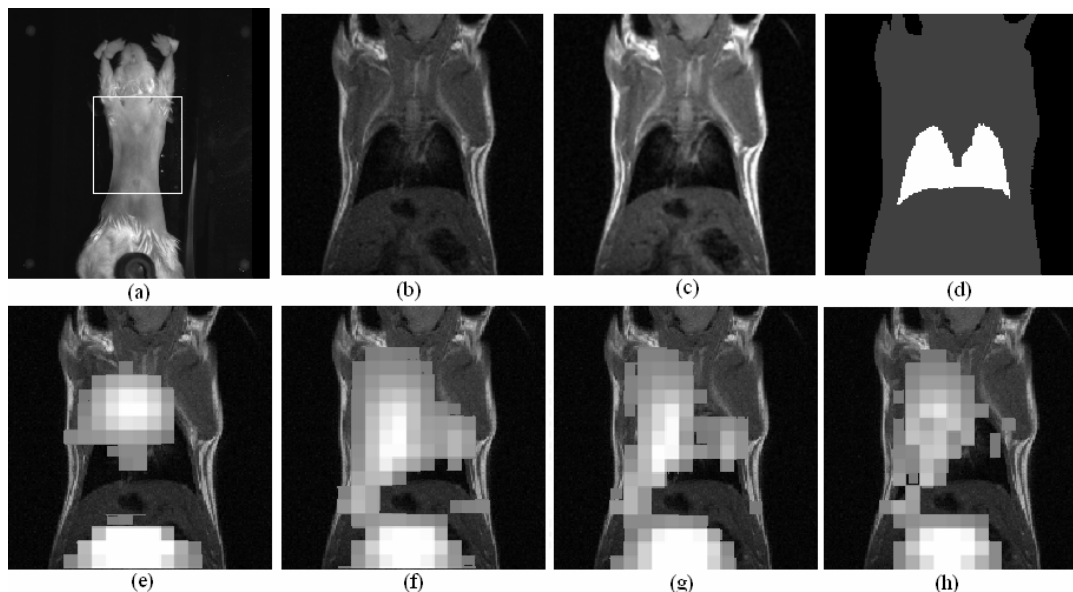


Fig. 1. (a) Photograph of the mouse. The white square box shows the field of view assumed in the studies. (b) The MR image sliced at depth 0.61 cm. (c) The preprocessed MR image sliced at depth 0.61 cm. (d) Segmented MR image. (e) Reconstructed image with $\lambda = 0$, no *a priori* information. (f) Image reconstructed with 0th order Tikhonov regularization where $\lambda = 0.08$. (g) Image reconstructed with 1st order Tikhonov regularization where $\lambda = 0.08$. (h) Image reconstructed with Tikhonov regularization where $\lambda = 0.08$, and \mathbf{L} is chosen according to the segmented anatomical image.

4. Discussions and Conclusion

The increased localization and contrast in fluorophore absorption coefficient reconstructions due to the incorporation of *a priori* information provided by a high-resolution anatomical imaging modality is shown through the experiments generated by a concurrent MRI/FMT imaging system and in-vivo measurements from mice. The prior information is incorporated by setting soft priors on the parameters sought in order to account for the possible mismatch between anatomical and molecular images. For this purpose, different Tikhonov regularization functions are compared, and it is concluded that 1st order regularization leads to better reconstructions for this experimental setup. As a further study, a hierarchical Bayesian approach to the inverse problem can be formulated where the regularization parameter and the prior image are taken as statistical parameters defined by some previously known hyperparameters so that the dependence of the reconstructions on the anatomical image is further reduced [11].

5. References

- [1] V. Ntziachristos, J. Ripoll, L. H. V. Wang, and R. Weissleder, "Looking and listening to light: the evolution of whole-body photonic imaging," *Nature Biotechnology* **23**, 313-320 (2005).
- [2] A. H. Hielscher, R. E. Alcouffe, and R. L. Barbour, "Comparison of finite-difference transport and diffusion calculations for photon migration in homogeneous and heterogeneous tissues," *Phys. Med. Biol.* **43**, 1285-1302 (1998).
- [3] V. Ntziachristos, C. Tung, C. Bremer, and R. Weissleder, "Fluorescence-mediated tomography resolves protease activity in vivo," *Nature Medicine*, **8**, 757-760 (2002).
- [4] R. B. Schulz, J. Ripoll, and V. Ntziachristos, "Experimental fluorescence tomography of tissues with noncontact measurements," *IEEE Trans. Med. Imaging* **23**(4), 492-500 (2004).
- [5] E. E. Graves, J. Ripoll, R. Weissleder, and V. Ntziachristos, "A submillimeter resolution fluorescence molecular imaging system for small animal imaging," *Med. Phys.* **30**(5), 901-911 (2003).
- [6] S. V. Patwardhan, S. R. Bloch, S. Achilefu, and J. P. Culver, "Time-dependent whole-body fluorescence tomography of probe biodistributions in mice," *Optics Express* **13**, 2564-2577 (2005).
- [7] M. J. Eppstein, D.E. Dougherty, D. J. Hawrysz, and E. M. Sevick-Muraca, "3-D Bayesian optical image reconstruction with domain decomposition," *IEEE Trans. Med. Imaging* **20**(3), 147-163 (2001).
- [8] J. C. Ye, K. J. Webb, C. A. Bouman, and R. P. Millane, "Optical diffusion tomography by iterative-coordinate-descent optimization in a Bayesian framework," *J. Opt. Soc. Am. A* **16**, 2400-2412 (1999).

- [9] V. Ntziachristos, A. G. Yodh, M. D. Schnall, and B. Chance, "MRI-guided diffuse optical spectroscopy of malignant and benign breast lesions," *Neoplasia* **4**, 347-354 (2002).
- [10] G. Gulsen, H. Yu, J. Wang, O. Nalcioglu, S. Merritt, F. Bevilacqua, A. J. Durkin, D. J. Guccia, R. Lanning, and B. J. Tromberg, "Congruent spectroscopy for functional and structural imaging of tumors," *Tech. in Cancer Res. & Treat.* **1**, 1 (2002).
- [11] M. Guven, B. Yazici, X. Intes, and B. Chance, "Diffuse optical tomography with anatomical *a priori* information," *Phys. Med. Bio.* **50**, 2837-2858 (2005).
- [12] A. Li, E. L. Miller, M. E. Kilmer, T. J. Brukilacchio, T. Chaves, J. Stott, Q. Zhang, T. Wu, M. Chorlton, R. H. Moore, D. B. Kopans, and D. Boas, "A tomographic optical breast imaging guided by 3D mammography," *Appl. Opt.* **42**, 5181-5190 (2003).
- [13] G. Alexandrakis, F. R. Rannou, and A. F. Chatziioannou, "Tomographic bioluminescence imaging by use of a combined optical-PET (OPET) system: a computer simulation feasibility study," *Phys. Med. Biol.* **50**, 4225-4241 (2005).
- [14] Q. Zhu, N. G. Chen, and S. H. Kurtzman, "Imaging tumor angiogenesis by use of combined near-infrared diffusive light and ultrasound," *Opt. Lett.* **28**, 337 (2003).
- [15] B. A. Brooksby, "Combining near infrared tomography and magnetic resonance imaging to improve breast tissue chromophore and scattering assessment," Ph.D. Dissertation, Dartmouth College, Hanover, New Hampshire (2005).
- [16] V. Kolehmainen, S. R. Arridge, W. R. B. Lionheart, M. Vauhkonen, and J. P. Kaipio, "Recovery of region boundaries of piecewise constant coefficients of an elliptic PDE from boundary data," *Inv. Prob.* **15**, 1375-1391 (1999).
- [17] A. X. Cong, and G. Wang, "A finite-element-based reconstruction method for 3D fluorescence tomography," *Opt. Soc. Am.* **13**(24), 9847-9857 (2005).
- [18] V. Ntziachristos, R. Weissleder, "Experimental three-dimensional fluorescence reconstruction of diffuse media by use of a normalized Born approximation," *Opt. Lett.* **26**(12), 893-895 (2001).
- [19] A. Soubret, J. Ripoll, and V. Ntziachristos, "Accuracy of fluorescent tomography in the Presence of Heterogeneities: study of the normalized Born ratio," *IEEE Trans. Med. Im.* **24**(10), 1377-1386 (2005).
- [20] M. Schweiger, S. R. Arridge, and I. Nissila, "Gauss-Newton method for image reconstruction in diffuse optical tomography," *Phys. Med. Biol.* **50**, 2365-2386 (2005).